Study of the Two-Dimensional Ising Model Using Computational Simulations

Nieto Pérez Marco, Sánchez-Toril Bastrygina Andrés, Ainoo Pérez Debinamaca, Molina O'Brien Marcos, Mompó Ruiz Lluís, Osa Bonillo Matilde, (Grupo 6)

[a]*Higher Technical School of Telecommunication Engineering, Valencia,*

Abstract

In this article, the analytical expressions for the average energy, magnetization, magnetic susceptibility, and specific heat per particle as a function of temperature are derived based on Lars Onsager's hypotheses about the model proposed by Ernest Ising. Subsequently, the validity of these calculations has been verified by computationally simulating a spin-lattice for cases where the external magnetic field is either null or has positive values. Finally, the results are discussed, pertinent conclusions are provided, and a general idea of the system's behavior is presented.

1. Context and Introduction

The Ising model is a problem originally formulated by physicist Wilhelm Lenz in 1920 and solved by his student Ernest Ising in his thesis in 1924 [1]. Its significance lies in being one of the first models exactly solved for an interacting system, describing ferromagnetism and phase transitions. Lars Onsager obtained the exact solution for the two-dimensional case in 1944 [2]. Today, its importance transcends statistical physics and has been applied to other areas such as biology.

2. Analytical Solution

derivation of the partition function for the two-dimensional Ising model requires a wide range of mathematical tools and, due to its length, will be developed in Appendix A. In that section, the analytical expression for $\ln Z/N$ is derived for the case where $J = 1$, which is identical — except for the notation — to equation (109b) presented by Lars Onsager in his article *Crystal Statistics. I. A two-dimensional model with an order-disorder transition * published in 1944 [2].

For our work, we will use as a starting point a more general expression for the case of a null external magnetic field [3], which essentially retains the same form as the derived equation.

$$Z = [\sqrt{2}\cosh(2K)]^N \exp\left[\frac{N}{\pi}\int_0^{\frac{\pi}{2}} \ln\left(1 + \sqrt{1-\kappa^2\sin^2(\phi)}\right)d\phi\right] \tag{1}$$

With $\kappa = 2\sinh(2K)/\cosh^2(2K)$ and $K = \beta J$. We calculate the internal energy, defined as $E = -\partial \ln Z/\partial\beta$ [4]. By interchanging the derivative with the integral, applying the chain rule, and differentiating the integrand with respect to κ before integrating with respect to ϕ, we arrive at the following expression for the energy per particle (E/N):

$$e = -2J\tanh(2K) + \frac{\kappa}{\pi}\left(\frac{\partial\kappa}{\partial\beta}\right)\int_0^{\frac{\pi}{2}} \frac{\sin^2(\phi)d\phi}{(1-\kappa^2\sin^2(\phi))\sqrt{1-\kappa^2\sin^2(\phi)}} \tag{2}$$

Rationalizing the integrand, the integral can be replaced by $(-\pi/2 + K_1(\kappa))/\kappa^2$, where $K_1(\kappa)$ is the complete elliptic integral of the first kind with modulus κ, defined as:

$$K_1(\kappa) = \int_0^{\pi/2} \frac{d\phi}{\sqrt{1-\kappa^2\sin^2\phi}}.$$

$$K_1(\kappa) = \int_0^{\pi/2} \frac{d\phi}{\sqrt{1-\kappa^2\sin^2(\phi)}} \tag{3}$$

Finding that: $(\partial\kappa/\partial\beta)/\kappa = 2J(\coth(2K) - 2\tanh(2K))$

We arrive at the following expression for the energy per particle as a function of the elliptic integral $K_1(\kappa)$:

$$e = -2J\tanh(2K) + \frac{2J}{\pi}(\coth(2K) - 2\tanh(2K))\left(\frac{-\pi}{2} + K_1(\kappa)\right) \tag{4}$$

By expanding $\coth(2K)$ and $\tanh(2K)$ in terms of $\cosh(2K)$ and $\sinh(2K)$, and applying the relation $\cosh^2(x) - \sinh^2(x) = 1$, we write the energy per particle in its final form:

$$e = -2J\tanh(2K) - \frac{J(\sinh^2(2K)-1)}{\cosh(2K)\sinh(2K)}\left(\frac{2}{\pi}K_1(\kappa) - 1\right) \tag{5}$$

The previous expression has been plotted as a function of temperature (see Fig. 1). The specific heat per particle can be calculated from the previous expression, considering $c = (\partial e/\partial T)$. Due to its length, it will not be included in this document, but its expression can be found in the code provided as an appendix, and its graph is shown in Fig. 1.

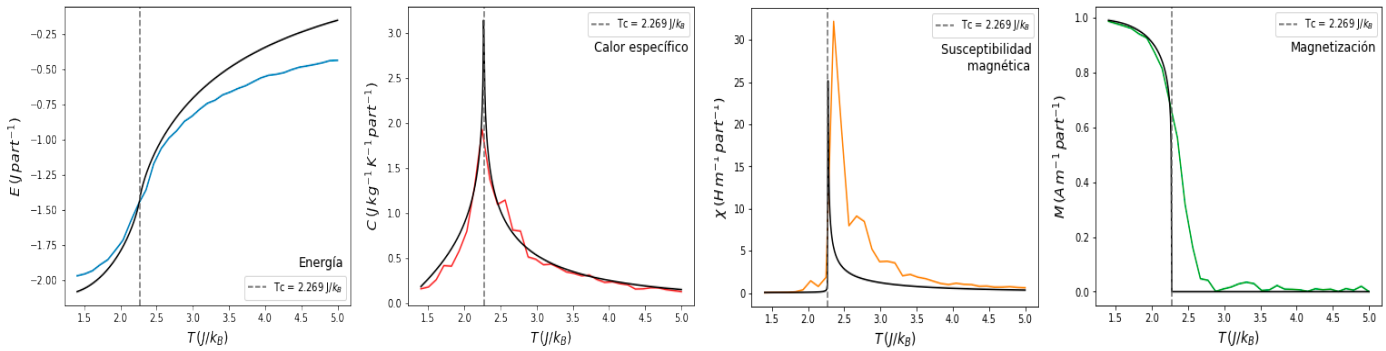

Figure 1: Dependencies of energy, specific heat, magnetic susceptibility, and magnetization with respect to temperature per particle. The abscissa corresponding to the theoretical critical temperature, $T_c = 2.269 J/k_B$, has been highlighted. The calculations were performed for a square spin lattice with a side length of $L = 20$, using a total of $700 \times N = 2.8 \times 10^5$ iterations.

Magnetization is defined as $M = -(\partial F/\partial B)$, where B is the magnetic field strength, the product of the magnetic permeability and the applied external field. For the two-dimensional Ising model, its expression was presented by Onsager in a lecture, but its derivation was not published. It was physicist C.N. Yang, Nobel Prize winner in Physics in 1957, who published an analytical derivation of this expression in 1952 [5]:

$$m(T) = \begin{cases} [1 - \sinh^{-4}(2K)]^{\frac{1}{8}} & \text{si } T \leq T_c \\ 0 & \text{si } T > T_c \end{cases} \tag{6}$$

where $T_c = 2/\ln(1+\sqrt{2}) \approx 2.269 J/k_B$.
For the case of magnetic susceptibility, χ, defined as $\chi = (\partial M/\partial B)$, studies have also been conducted, and bibliographic articles have determined its expression. It can be written as [4][6]:

$$\chi(T) = \frac{N\mu^2}{k_B T_c} \times \begin{cases} C_- \left[\frac{|T-T_c|}{T_c}\right]^{\frac{-7}{4}} & \text{si } T \leq T_c \\ C_+ \left[\frac{T-T_c}{T_c}\right]^{\frac{-7}{4}} & \text{si } T > T_c \end{cases} \tag{7}$$

Where C_+ and C_- take the values 0.96258 and 0.02554, respectively. Both quantities have been plotted as a function of temperature (see Fig. 1).
It is worth mentioning that, unlike the one-dimensional case, there are no analytical expressions for the aforementioned quantities when an external magnetic field H is applied, so their determination can only be achieved through numerical simulations.

3. Computational Simulations

To simulate the behavior of a spin lattice, the Metropolis-Hastings algorithm [7] was used. It involves starting with a random initial configuration ($\sigma_i = \pm 1$) and, in each iteration of the method, modifying the value of a randomly selected spin. After recalculating the energy variation due to this change, if $\Delta E \leq 0$, the change is accepted; if $\Delta E > 0$, the change is accepted with a probability $p = e^{-\beta \Delta E}$. These iterations are repeated a sufficiently large number of times so that the system explores a significant portion of the configurations in its associated phase space.

The numerical calculation of the expressions is performed identically to the one-dimensional case. The expressions were already derived in a previous work [8], so in this case we will limit ourselves to presenting them and highlighting the differences to be considered here.

3.1. Average Magnetization

We computationally estimate the system's magnetization as:

$$\overline{M} = \frac{1}{n} \sum_{K=1}^{n} \sum_{i=1}^{N} \sigma_i^{(K)}$$

Where N is the total number of spins, n the number of iterations of the method, $K = 1, 2, ..., n$ the number of tested configurations, and $\sigma_i^{(K)}$ the value of spin i in configuration K. In the two-dimensional case, instead of taking each spin as elements of a list, they must be considered as elements of a matrix of size $L \times L$. An estimate of the magnetization as a function of temperature has been obtained (see Fig. 1). The case where the external field is non-zero is calculated in the same way (see Fig. 2).
Additionally, the spin configuration has been plotted for four different time points: before starting the iterations (initial configuration), after 1/10 of the Monte Carlo iterations, after 1/2 of the iterations, and finally the final configuration. The evolution has been graphed for the system at two different temperatures: one below T_c ($T < 2.269$) and the other above T_c ($T > 2.269$) (see Fig. 3).

3.2. Average Energy

The expression for the average energy can be written as:

$$\overline{E} = \frac{1}{n} \sum_{K=1}^{n} H_{(H=0)}^{(K)}$$

For the two-dimensional case, the Hamiltonian in each iteration takes the form [9]:

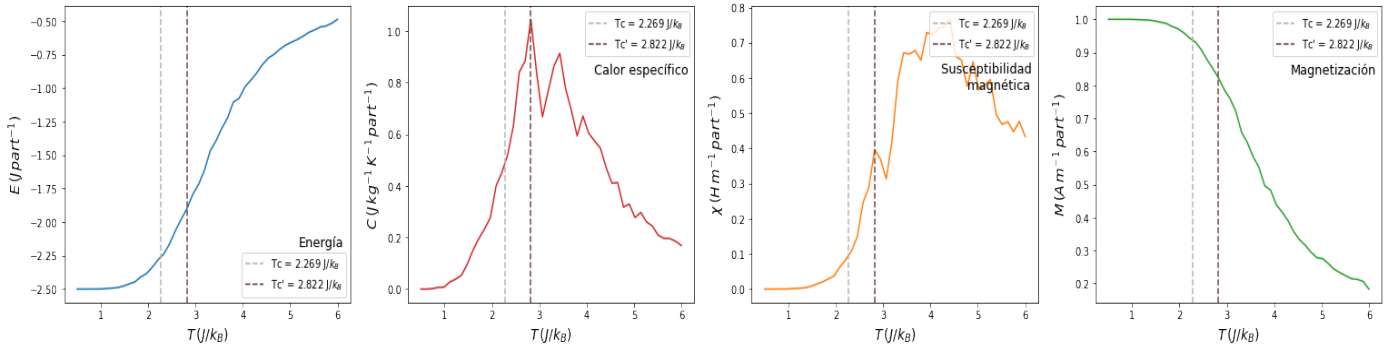

Figure 2: Dependencies of energy, specific heat, magnetic susceptibility, and magnetization with respect to temperature per particle for an external field $H = 0.5$. The abscissa corresponding to the theoretical critical temperature, as well as an estimate for the new critical temperature, has been highlighted. The calculations were performed for a square spin lattice with a side length of $L = 20$, using a total of $700 \times N = 2.8 \times 10^5$ iterations.

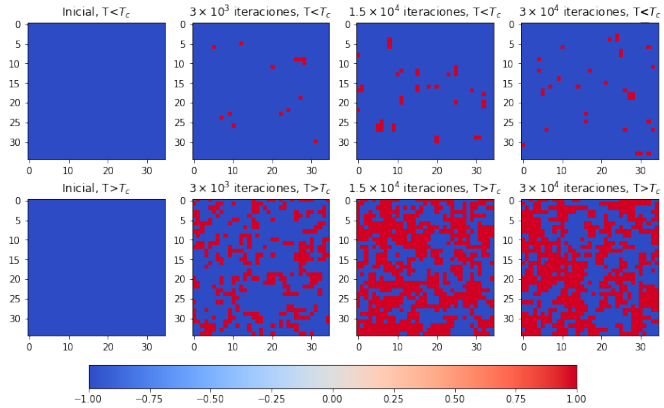

Figure 3: Spin configuration throughout the iterations, starting from a lattice of aligned spins for a value of $T < T_c$ (top row) and for a value of $T > T_c$ (bottom row). The graph was generated using a lattice of $L = 35$ and 3×10^4 iterations.

$$H^{(K)}_{(H=0)} = -J\left[\sum_i^L \sum_j^L \sigma^{(K)}_{i,j}\sigma^{(K)}_{i+1,j} + \sum_i^L \sum_j^L \sigma^{(K)}_{i,j}\sigma^{(K)}_{i,j+1}\right] \quad (8)$$

Where $\sigma^{(K)}_{i,j}$ is the spin value in row i and column j of the matrix in configuration K. An approximation of the average energy curve as a function of temperature has been obtained (see Fig. 1). For the case where an external field H is introduced, the term $-H\sum_i\sum_j \sigma^{(K)}_{i,j}$ must be added to the previous Hamiltonian. Once again, the temperature dependence has also been plotted for this case (see Fig. 2).

3.3. Heat capacity

The heat capacity can be calculated as:

$$\overline{C} = \frac{1}{k_B T^2}\left[\left(\frac{1}{n}\sum_{K=1}^n H^{(K)\,2}_{(H=0)}\right) - \left(\frac{1}{n}\sum_{K=1}^n H^{(K)}_{(H=0)}\right)^2\right]$$

The result of the above expression has been multiplied by N for normalization, as calculating it as the fluctuation of another parameter introduces a $1/N$ factor that causes it to differ from the analytical curve. As with the two previous parameters, its dependence on temperature has been determined (see Fig. 1, Fig. 2).

3.4. Magnetic Susceptibility

The expression for calculating magnetic susceptibility can be written as:

$$\overline{\chi} = \frac{1}{k_B T}\left[\frac{1}{n}\sum_{K=1}^n\left(\sum_{i=1}^N \sigma^{(K)}_i\right)^2 - \left(\frac{1}{n}\sum_{K=1}^n\sum_{i=1}^N \sigma^{(K)}_i\right)^2\right]$$

As with heat capacity, its expression has been normalized with a factor N, and the numerical approximation of its dependence on temperature has been determined for both the null and non-zero external magnetic field cases (see Fig. 1, Fig. 2).

For the case with a non-zero external magnetic field, a new critical temperature has been estimated at the abscissa value where the heat capacity reaches its maximum. This temperature is purely indicative and should not be considered as the result of a rigorous calculation, as, as observed and discussed later, the system would require many more iterations and computational capacity for the numerical trends to perfectly match the analytical ones.

4. Discussion of Results

This section presents the discussion of the results obtained from the computational simulations of the two-dimensional Ising Model and compares them with the results from the simulation of the one-dimensional Ising Model. A detailed explanation of the system's behavior will be omitted as it was already provided in our previous work on the one-dimensional Ising Model [8].

4.1. Without Field (fig. 1)

4.1.1. Average Energy

As observed in the graph, energy increases as the system's temperature rises, showing behavior similar to the analytical graph. The increase in energy with temperature is intuitive since, as temperature rises, atomic motion increases, contributing more

energy to the system.

The main difference between the 2D and 1D Ising models is that, due to a greater number of interactions, the average energy starts from a higher absolute value. Additionally, the maximum energy variation coincides with the critical temperature, but in this case, the maximum occurs at a higher temperature because the critical temperature is higher. Nevertheless, the behavior is similar, as it also converges to 0.
In this graph, it can be seen that the energy does not entirely match the theoretical values, due to computational limitations in this study, as the 2D Ising model requires a much larger number of particles and iterations than the 1D Ising model. However, these results are still useful for explaining and analyzing this quantity's behavior since, despite not matching exact values, the trend is the same.

4.1.2. Specific Heat

Specific heat is the variation of average energy with respect to temperature. Looking at the graph, it is observed that the value is maximum precisely at the critical temperature, i.e., when the system undergoes a phase transition. This is because, at this temperature, the variation in average energy per particle is maximal.
The main difference between the two models is that in the 2D Ising model, the maximum specific heat value is more pronounced due to the phase transition. Conversely, in the 1D model, there is no phase transition (although the maximum represents where it would occur); it is smoother than in the 2D case, and the values are smaller. This occurs because, in 1D, spins interact only with nearest neighbors, limiting the energy. Meanwhile, in 2D, spins interact with neighbors in all directions, forming more complex structures and spatial configurations, resulting in a broader and more varied energy distribution. This causes greater energy fluctuations, leading to higher specific heat values compared to the 1D case.

4.1.3. Magnetic Susceptibility

The behavior of magnetic susceptibility is similar to that of specific heat. This quantity indicates how susceptible a material is to being magnetized. Since it is calculated from magnetization fluctuations, it peaks precisely in the region where magnetization begins to decay, i.e., during the phase transition.
The main difference with the 1D Ising model is that, since the phase transition occurs at a higher critical temperature, the maximum susceptibility value shifts to a higher critical temperature. Additionally, there is a significant difference in magnitude. In the 2D model, susceptibility is much higher due to the increased number of neighbors with which a spin interacts, meaning the magnetic moment is influenced by a greater number of neighboring fields, making it more susceptible to magnetization. Note also that the change in susceptibility is very abrupt, whereas in the 1D model, the decline was more gradual. This behavior occurs because the 1D model forced a phase transition that did not occur. In the 2D model, a physical phase transition exists, which is modeled accordingly. Moreover, since susceptibility is calculated from magnetization fluctuations, and magnetization shows its maximum variation at the critical temperature—where the graphs exhibit a slope of 90°—the maximum susceptibility value is observed at this point, followed by a progressive decline consistent with the drop in magnetization.

4.1.4. Magnetization

The behavior of magnetization is one of decay at a certain temperature, specifically the critical temperature or Curie temperature. This marks the moment of phase transition, from ferromagnetic to paramagnetic.
The difference is that in the 2D model, the drop occurs at a higher temperature since the critical temperature is higher. The behavior in both models is the same: upon surpassing the critical temperature, magnetization drops to 0, meaning the material becomes paramagnetic.

4.2. With Field (fig. 2)

4.2.1. Average Energy

The system's behavior is identical to the no-field case. However, as seen, the initial energy is higher in absolute value than in the $H = 0$ case. This is because adding an external field causes the spins to interact with it, increasing their internal field, and thus, each spin's energy increases in absolute value. In this case, it can be observed that, with the critical temperature shifted, energy remains constant at higher temperatures compared to the no-field case, as it becomes more difficult to misalign the spins in the presence of this magnetic field.
Compared to the 1D case, the fundamental difference is the temperature at which the energy begins to converge to 0, the point at which the system is in equilibrium. This is because, in 2D with a field, the critical temperature shifts to much higher values than in 1D with a field.

4.2.2. Specific Heat

Adding an external magnetic field increases the critical temperature, meaning the phase transition occurs at a higher temperature. Consequently, the maximum appears shifted compared to the no-field case. As observed, the values are lower than in the no-field case because the presence of an external magnetic field causes the spins to align with it, reducing the energy fluctuations associated with maintaining alignment. Since specific heat is proportional to these fluctuations, its reduction leads to lower values for this quantity. The behavior is equivalent to the 1D case.

4.2.3. Magnetic Susceptibility

Adding a magnetic field increases the critical temperature, so the maximum magnetic susceptibility value is shifted. Regarding the maximum value, it is lower with a field than without because the presence of an external field makes the material less susceptible to being magnetized due to its pre-existing magnetization. This is why achieving maximum randomness in the spin orientations requires higher temperatures. As the field becomes larger, the material becomes less susceptible to further magnetization. On the other hand, compared to the no-field case, susceptibility tends to 0 more slowly after the maximum. This

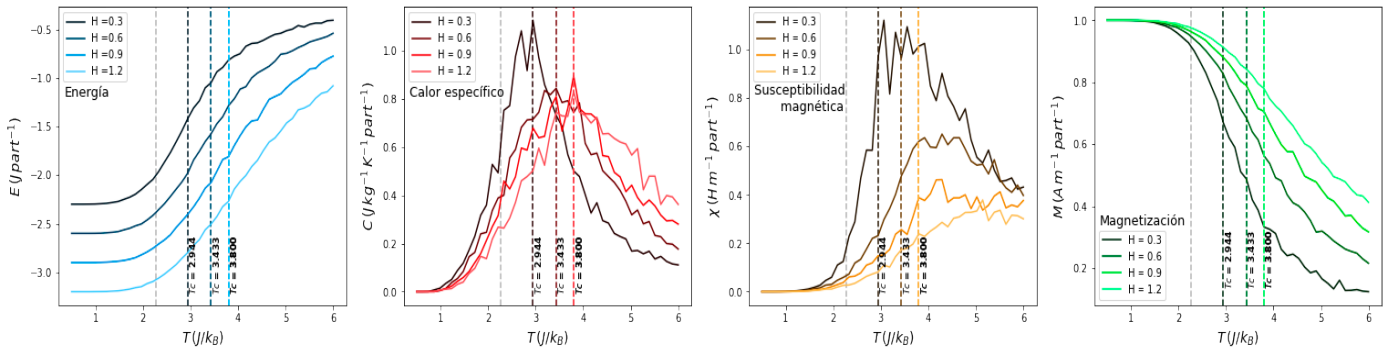

Figure 4: Dependencies of energy, specific heat, magnetic susceptibility, and magnetization on temperature per particle for different external field values. The abscissa of the critical temperature for the zero external field case has been highlighted, along with estimates for the new critical temperatures with $h \neq 0$. Calculations were performed for a square spin lattice with side $L = 17$ and a total of $500 \times N \approx 1.5 \times 10^5$ iterations. The resulting critical temperatures were 2.944, 3.433, 3.800, and 3.800 J/k_B for $H = 0.3, 0.6, 0.9$, and 0.12, respectively.

is because magnetization is not reduced as abruptly as in the no-field case, and the phase transition occurs more gradually, controlled by the external field that keeps the spins aligned. As with specific heat, the behavior is analogous to the 1D case.

4.2.4. Magnetization

Adding a magnetic field causes the spins to align with it and maintain that position. This means higher temperatures are needed to misalign them, and the phase transition does not occur as abruptly as in the no-field case, so the decline in magnetization is slower. Therefore, more temperature is needed to transition from ferromagnetic to paramagnetic. Comparing the fourth graph in Fig. 2 with that in Fig. 1, we can see that magnetization tends to zero at a higher temperature, indicating that the critical temperature is higher when an external magnetic field is present. It is evident that the behavior is analogous to the 1D case with a field.

5. Study of System Behavior

This section details how the variation of certain parameters affects the results and explores different ways of observing the system's behavior.

5.1. Variation of External Magnetic Field

The magnitudes discussed in the previous section have been plotted for different external field values (see Fig. 4). Similarly to Fig. 2, a critical temperature has been estimated for each value of H, placing the figure on the abscissa where the specific heat is maximal. This value is purely indicative and aims only to show how, in general, T_c shifts to higher temperatures as the external field H increases.

First, regarding energy, we see that with a greater external magnetic field, the initial energy is higher in absolute value since this field interacting with the spins adds energy to them. Physically, spins tend not to move due to the presence of the mean field, requiring higher temperatures to reach energy equilibrium at 0.

Second, specific heat does not vary much with different external magnetic fields. The behavior is qualitatively the same, with the only difference being the point at which the maxima are reached, as the critical temperature shift delays the occurrence of maximum energy fluctuations. On the other hand, the maxima of this quantity are lower with higher magnetic fields because the energy fluctuations are reduced by the tendency of spins to align with the field, as explained in the previous section. Since this quantity depends on energy fluctuations, its maximum decreases.

Regarding magnetic susceptibility, its peak decreases as the magnetic field increases, as the material becomes less likely to magnetize with a stronger field. The behavior remains the same for all cases, tending to 0 following Curie's law. However, as with specific heat, its maxima appear at higher temperatures as the magnetic field increases because the magnetization fluctuations are reduced by the tendency of spins to remain parallel to the external field.

Finally, regarding average magnetization, for very low fields we see how it quickly tends to 0 with a steeper slope. This decline is smoother as the critical temperature shifts, due to the increased difficulty of misaligning the spins under the influence of their mean field. That is, the influence of the field from neighboring spins makes it harder for them to misalign, causing the phase transition to occur more slowly and at sufficiently high temperatures for thermal energy to dominate over that generated by the external field, as explained in the previous section.

5.2. Variation in the Number of Particles

The dependence of specific heat and magnetic susceptibility on T has been plotted for different values of L, as these two quantities exhibit peaks that should tend to infinity and pose the greatest difficulty in converging to their analytical expressions (fig. 5). In the simulations, we observe what happens when the number of particles is varied while keeping the number of iterations constant. It can be seen that as the number of particles increases, the error with respect to the theoretical value

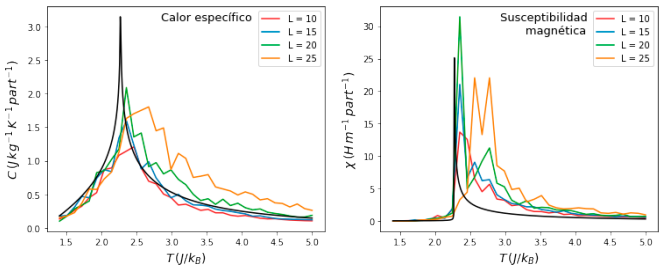

Figure 5: Different numerical approximations (normalized by a factor N) for different values of L, with the same number of iterations: 1.125×10^5.

grows due to the relationship between the number of particles and iterations. We can conclude that obtaining optimal results requires the number of iterations to be much greater than the number of particles. On the other hand, increasing the number of particles helps smooth the computed curve, showing less pronounced fluctuations. However, as observed, increasing the number of particles is detrimental to achieving a good approximation if this increase is not accompanied by a much larger number of iterations.

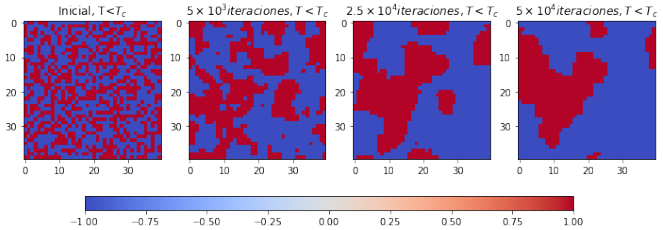

Figure 6: Variation of the lattice over iterations starting from a random configuration for a value of $T < T_c$. The graph was generated with a lattice of $L = 40$ and 5×10^4 iterations.

5.3. Magnetic Domains

A magnetic domain is a region within a material with uniform magnetization, i.e., regions where magnetic moments are aligned. In the 2D Ising model, magnetic domains appear for temperatures below the critical one because this is the range where the intrinsic energy of alignment dominates over thermal energy. At temperatures above the critical point, the system transitions to a random spin distribution (see fig. 3). Starting from a random configuration at a fixed temperature below the critical point, spins tend to align parallel to each other (see fig. 6). If a spin is misaligned within a group of aligned spins, they will exert influence for the misaligned spin to adopt the group's orientation. As iterations progress, new spins are added to each group, generating clusters that tend to expand throughout the domain. If the temperature is increased beyond the critical point, thermal energy becomes significant, leading to more spin fluctuations and greater disorder (as seen in fig. 3), resulting in smaller or disappearing magnetic domains.

These domains form whether the initial spin distribution is random or mostly aligned. However, a greater number of iterations is needed in cases where spins are initially mostly aligned because, at low temperatures, randomness is minimal, making it harder for spins to change orientation (see fig. 3). Thus, in such cases, the formation of these domains is slower, appearing in smaller dimensions and more sporadically.

In the 1D Ising model, these domains cannot be observed because the spins are distributed linearly, preventing the generation of these regions.

5.4. Hysteresis

Hysteresis refers to a material's tendency to retain magnetization M after the external magnetic field H is removed. Three hysteresis cycles at different temperatures have been plotted (see fig. 7). Note that at lower temperatures, due to less variation in spins, saturation magnetization is achieved with a smaller magnetic field. Conversely, at temperatures closer to the critical point, there is greater spin variation, requiring a stronger external magnetic field to reach saturation magnetization. On the other hand, it is observed that the hysteresis loop's area is larger at lower temperatures. This makes sense since at low temperatures, spin fluctuations are rare, making it much harder to reduce magnetization after removing the field. In other words, the spins tend to remain parallel, explaining why saturation magnetization persists during magnetic field variations. However, at higher temperatures near the critical point, the loop's area is smaller because, with thermal energy playing a significant role, it becomes easier for spin orientation to change, causing magnetization to quickly decrease as the magnetic field is reduced.

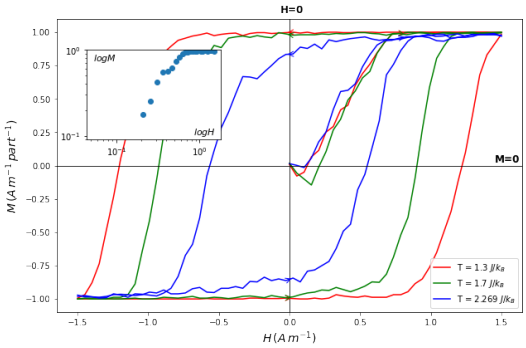

Figure 7: Dependence of magnetization on the applied external field H, starting from random configurations with zero field. Results for a lattice with side $L = 25$. LogM versus logH has been plotted for the range $H \in [0, 1.5]$, for the case where $T = T_c$.

In the 1D Ising model, this behavior would not occur because ferromagnetic behavior does not appear, and removing the external magnetic field would cause the spins to fluctuate rapidly. This is because in 1D, spins interact only with their nearest neighbors, resulting in less influence among spins. At low temperatures, they would also fluctuate because they are less influenced than in 2D, where we have a more complex distribution and interactions between multiple spins.
Additionally, the dependence of log$M$ versus log$H$ has been plotted for H values between 0 and H_{max}, i.e., 1.5, for the

case where the temperature equals the critical temperature. This was done to approximate the critical exponent δ, but due to limited computational capacity, we could not achieve a coherent result. For this reason, the graph has been left as supplementary information without arriving at a numerical value for the exponent.

Theoretically, however, it is known that the critical exponent δ in the 2D Ising model takes a value of $\delta = 15$ [10]. This critical exponent refers to the relation known as the critical isotherm ($M = H^{1/\delta}$). Determining δ provides information on how the system's magnetization responds to the applied magnetic field near the critical point of the phase transition.
In general, obtaining critical exponents such as α, β, or γ for specific heat, magnetization, and initial susceptibility, respectively, is key to describing the behavior of thermodynamic variables when a magnetic system, in this case, is near the critical temperature. Additionally, it is worth noting that the value of these exponents varies depending on the type of system studied. In real systems, they may also depend on factors such as magnetic interactions or material structure.

6. Conclusions

As demonstrated in the computational simulations section, the Metropolis algorithm is an effective method for approximating the 2D Ising model. Unlike the 1D model, the 2D model exhibits a phase transition, so no oscillations occur near the critical temperature. This is because, in the 1D model, the critical temperature is 0 or very close to 0, and dividing by this value causes significant variations in the results. The physical sense of the trends in the different quantities has been thoroughly discussed in the results discussion section. Additionally, while plotting the results, it was concluded that beyond a certain number of particles, increasing the number of steps is more important than increasing the number of particles to achieve accurate approximations.

Moreover, the 2D Ising model provides greater depth in explaining real magnetic behaviors that the 1D Ising model cannot explain due to its simplicity. For instance, magnetic domains, discussed in the previous section, help explain phenomena such as metastability. Metastability refers to the existence of metastable states in a system that can persist for a significant time before reaching equilibrium. Domains act as these metastable states, where regions with opposite spin orientations coexist and persist before reaching equilibrium. The 2D Ising model also provides insights into nucleation, the process by which a new magnetic domain forms within a system. This process originates from configuration changes below the critical temperature, which were observed in the previous section. Additionally, we verified that this model is ideal for explaining ferromagnetic material behavior through hysteresis cycles and even in determining critical exponents to describe their behavior.

In conclusion, the Ising model has proven to be a key study for explaining numerous real magnetic phenomena and its importance in physics.

Appendix A. Derivation of the Partition Function

We start by considering a discrete lattice with side length L, where each point hosts an ideal spin with a value of ± 1 (a total of $N = L^2$ spins). We identify two specific positions with the subscripts $i, j = 1, 2, \ldots, L^2$. Unlike the 1D case, where each spin had two immediate neighbors, in the 2D case, each particle has four immediate neighbors. We denote with the symbol $\mathcal{N}$ the set of pairs of points (i, j) such that the spins σ_i, σ_j are immediate neighbors. Thus, we define the system's Hamiltonian as:

$$H = -J \sum_{i,j \in \mathcal{N}} \sigma_i \sigma_j \tag{A.1}$$

Here, J is the coupling constant, and the summation does not double-count contributions from the pair (j, i) if the pair (i, j) has already been considered. Without loss of generality, we set the coupling constant to 1. We define the partition function as $Z = \sum_\sigma e^{-\beta H}$, where $\beta = 1/k_B T$ and $\sum_\sigma = \sum_{\sigma_1=\pm 1} \sum_{\sigma_2=\pm 1} \cdots \sum_{\sigma_N=\pm 1}$. Since the partition function expression involves a summation within the exponential term, we rewrite it using a product:

$$Z = \sum_{\sigma_1=\pm 1} \sum_{\sigma_2=\pm 1} \cdots \sum_{\sigma_N=\pm 1} \prod_{\mathcal{N}} e^{\beta \sigma_i \sigma_j} \tag{A.2}$$

Considering that $\sigma_i \sigma_j = \pm 1$ and $\exp(\pm x) = \cosh(x) \pm \sinh(x)$, we find that $\exp(\beta \sigma_i \sigma_j) = \cosh(\beta)(1 + \sigma_i \sigma_j u)$, where $u = \tanh(\beta)$. Using the relation $1 - \tanh^2(x) = \operatorname{sech}^2(x)$ and applying the variable substitution $u = \tanh(\beta)$, we determine the relationship between cosh and u, $\cosh(\beta) = 1/\sqrt{1 - u^2}$. With these considerations, we rewrite the partition function as:

$$Z = \sum_{\sigma_1=\pm 1} \sum_{\sigma_2=\pm 1} \cdots \sum_{\sigma_N=\pm 1} \prod_{\mathcal{N}} \frac{(1 + \sigma_i \sigma_j u)}{\sqrt{1 - u^2}} \tag{A.3}$$

Assuming periodic boundary conditions, the total number of links, n_b, equals $2N$. We can factor the root term outside the product and summations, rewritten as $(1-u^2)^{-n_b/2} = (1-u^2)^{-N}$. Next, we expand the term $\prod_{\mathcal{N}}(1 + \sigma_i \sigma_j u)$. Expanding it as $(1 + \sigma_{i1} \sigma_{j1} u)(1 + \sigma_{i2} \sigma_{j2} u) \ldots$, we observe that this product can be synthesized as $\sum_{m=0}^{2N} u^m \prod_{\mathcal{N}^m} \sigma_{im} \sigma_{jm}$, where the summation spans each of the $2N$ possible links (denoted by m).
In graph theory terms, the above summation traverses all graphs with m edges (i.e., m links). We note that if a node σ_k has degree q_k in a particular graph with m edges, σ_k will appear q_k times in the product of graphs with m edges (thus, a term σ^{q_k} appears). If any node has an odd degree, its contribution will be null in the spin summation because $\sum_{\sigma_k=\pm 1} \sigma^{q_k} = -1 + 1 = 0$, eliminating the entire graph's contribution to the partition function. Hence, only graphs with nodes of even degree contribute, each with a factor of 2 per node since $\sum_{\sigma_k=\pm 1} \sigma^{q_k} = 1 + 1 = 2$. If the graph has V vertices, it contributes a factor of 2^V. Additionally, we

must account for the $N - V$ spins that are not part of the graph ($q_k = 0$), contributing another factor of 2. Thus, the graph's total contribution is $2^{V+N-V} = 2^N$. Separating the $m = 0$ term (equal to 1), we rewrite the original product as $\prod_{\mathcal{N}}(1+\sigma_i\sigma_j u) = 1 + \sum_{m=1}^{2N} u^m \prod_{\mathcal{N}^m} \sigma_{im}\sigma_{jm}$.
The partition function expression then becomes:

$$Z = 2^N(1-u^2)^{-N}\left(1 + \sum_{G\in\mathcal{A}} u^{m(G)}\right) \tag{A.4}$$

Here, $\mathcal{A}$ represents the set of all admissible graphs, and $m(G)$ is the number of links in the admissible graph G. Since no nodes have odd degrees, none will terminate a spin chain, and the graph can be decomposed into closed paths. Additionally, the links are directed (a link i, j starts from spin i and ends at j). The sign of a path p is defined as:

$$s(p) = -(-1)^{\omega t} \tag{A.5}$$

Here, t is the total rotation angle divided by 2π (with positive angles defined counterclockwise), and ω is equal to 1 for non-periodic paths and the largest integer such that ω identical sub-paths are not periodic in the case of a periodic path.
The path amplitude is defined as:

$$W(p) = s(p)u^{m(p)} \tag{A.6}$$

where m is the total length of the path. It can be shown that $1 + \sum_{G\in\mathcal{A}} u^{m(G)} = \prod_{[p]}(1 + W(p))$, where $[p]$ denotes the set of non-periodic closed paths. Using this relationship, we rewrite the partition function as:

$$Z = 2^N(1-u^2)^{-N}\prod_{[p]}(1 + W(p)) \tag{A.7}$$

Next, we detail the accounting of paths. Since the sign of a path depends on the angle rotated at each step, right or left turns contribute a factor of 1/4 to the change in sign. We define the left-turn factor as $\alpha = e^{i\pi/4}$, and similarly, the right-turn factor as $\bar{\alpha} = e^{-i\pi/4}$. For going straight, this factor is assigned the value 1, and for going backward, it is assigned the value 0. Using these factors, the path amplitude can be rewritten as $W(p) = \bar{\alpha}^a\alpha^b 1^c 0^d u^{a+b+c+d}$, where a is the number of right turns, b the number of left turns, c the number of straight steps, and d the number of backward steps. Similar to probability theory, wave mechanics, or quantum mechanics, we assume that amplitudes obey the principle of linear superposition, i.e., the combined amplitude of a set of paths equals the sum of the amplitudes of each path. Considering positive y values as the upward direction (U) and positive x values as the rightward direction (R), the amplitude for arriving from below (direction U) in step n at the point (x, y) is given by $U_n(x, y) = [U_{n-1}(x, y-1) + 0D_{n-1}(x, y-1)+\alpha L_{n-1}(x, y-1)+\bar{\alpha}R_{n-1}(x, y-1)]u$, (D denotes the downward direction, and L the leftward direction). Expressions for $D_n(x, y)$, $L_n(x, y)$, and $R_n(x, y)$ are obtained similarly. Therefore, the total amplitude for all possible segments starting from an arbitrary origin and reaching the point (x, y) after exactly n steps is $U_n(x, y) + D_n(x, y) + L_n(x, y) + R_n(x, y)$. This amplitude can be expressed as a recurrence relation involving terms from $n-1$ and earlier, which implies a shift in our lattice. To simplify these spatial translations and convert them into phase shifts, we employ the two-dimensional Fourier transform and its inverse, defined as [11]:

$$\hat{U}_n(k_x, k_y) = \sum_{x=-\infty}^{\infty}\sum_{y=-\infty}^{\infty} U_n(x, y)e^{-ik_x x}e^{-ik_y y} \tag{A.8}$$

$$U_n(x, y) = \int_0^{2\pi}\int_0^{2\pi} \hat{U}_n(k_x, k_y)e^{ik_x x}e^{ik_y y}dk_x dk_y \tag{A.9}$$

Applying the transform to $U_n(x, y)$, we find that $\hat{U}_n(k_x, k_y) = ue^{-ik_y}[\hat{U}_n(k_x, k_y)+0\hat{D}_n(k_x, k_y)+\alpha\hat{L}_n(k_x, k_y)+\bar{\alpha}\hat{R}_n(k_x, k_y)]$. Transforms for the other three amplitudes are obtained analogously. Defining the vector $\psi_n = [\hat{U}_n, \hat{D}_n, \hat{L}_n, \hat{R}_n]$ and the matrix

$$M = \begin{bmatrix} v & o & v\alpha & v\bar{\alpha} \\ 0 & \bar{v} & \bar{v}\bar{\alpha} & \bar{v}\alpha \\ \bar{h}\bar{\alpha} & \bar{h}\alpha & \bar{h} & 0 \\ h\alpha & h\bar{\alpha} & 0 & h \end{bmatrix} \tag{A.10}$$

Where $v = e^{-ik_y}$ and $h = e^{ik_x}$. We express the recurrence relation as $\psi_n = uM\psi_{n-1} = u^n M^n\psi_0$. Observe that for a closed cycle, $\psi_n = \psi_0$. Defining ϵ_i with $i = 1, 2, 3, 4$ as the unit vectors forming the basis of ψ (directions U, D, R, L), the Fourier-transformed expression for the amplitude of all paths ending at the origin with direction U (closed paths) is $u^n\psi_0^T M^n\psi_0$ with $\psi = \epsilon_1$. Thus, the contributions of the four possible directions to the total amplitude can be written as:

$$\sum_{i=1}^{4}\langle\epsilon_i|(uM)^n|\epsilon_i\rangle = \mathrm{Tr}(uM)^n \tag{A.11}$$

Where the notation for transposed vectors in the first expression has been simplified using Dirac's Bra-Ket notation. Undoing the Fourier transform, we arrive at the expression for the final amplitude:

$$\sum_{n=1}^{\infty}\frac{1}{n}\sum_{p(n)} W(p) = \sum_{n=1}^{\infty} -\frac{N}{2n}\frac{1}{(2\pi)^2}\int_0^{2\pi}\int_0^{2\pi}\mathrm{Tr}(uM)^n dk_x dk_y \tag{A.12}$$

First, a factor $\sum_{n=1}^{\infty} 1/n$ has been added because for a given path of length n, there are n possible initial positions, which eliminates previously considered terms. Second, since the amplitude's sign is -1 times the number of times the path's tangent vector rotates around the origin, it was necessary to multiply by -1. Additionally, we have only considered paths starting and ending at a specific origin, so we must multiply the expression by N to account for all possible origins and divide by a factor of 2 since counting the path in the reverse direction is redundant. It can be shown that interchanging the order of integrals and summation is valid. Thus, we can perform this interchange and rewrite $\mathrm{Tr}\sum_{n=1}^{\infty} -(uM)^n/n = \mathrm{Tr}\ \ln(1 - uM) = \ln\det(1 - uM)$. Note that $\sum_{n=1}^{\infty} 1/n\sum_{p(n)} W(p)$ is equivalent to $\sum_{[p]}(W - W^2/2 + W^3/3 - \cdots) = \sum_{[p]} ln(1+W) = \ln\prod_{[p]}(1+W)$. In both cases, the sum of logarithms has been applied as the logarithm of the product. Returning to our variable change,

$u = \tanh(\beta)$, and applying certain trigonometric relations, it can be shown that $\ln \det(1 - uM) = -4 \ln \cosh(\beta) + \ln[\cosh^2(2\beta) - \sinh(2\beta)(\cos(k_x) + \cos(k_y))]$ and that $1 - u^2 = 1/\cosh^2(\beta)$. Combining the above expressions, we finally rewrite the partition function as:

$$Z = [2\cosh^2(\beta)]^N \exp\left[\frac{N}{2n}\frac{1}{(2\pi)^2}\int_0^{2\pi}\int_0^{2\pi} \xi dk_x dk_y\right] \quad \text{(A.13)}$$

Where $\xi = -4 \ln \cosh(\beta) + \ln[\cosh^2(2\beta) - \sinh(2\beta)(\cos(k_x) + \cos(k_y))]$.

From this, the expression for $\ln Z/N$ is derived:

$$\ln[2\cosh(2\beta)] + \frac{1}{2\pi^2}\int_0^{\pi}\int_0^{\pi} ln[1 - 2\kappa(\cos(k_x) + \cos(k_y))]dk_x dk_y \quad \text{(A.14)}$$

Where $2\kappa = \sinh(2\beta)/\cosh^2(2\beta)$.

References

[1] Ernst Ising. Beitrag zur theorie des ferromagnetismus - zeitschrift für physik a hadrons and nuclei, Feb 1925.

[2] Lars Onsager. Crystal statistics. i. a two-dimensional model with an order-disorder transition. *Phys. Rev.*, 65:117–149, Feb 1944.

[3] J. Ricardo Arias-Gonzalez. Práctica informática de física estadística 6: Modelo de ising 2d y transiciones de fase. 2023.

[4] Paul D. Beale R.K. Pathria. *Statistical Mechanics*. Katey Birtcher, 4 edition, 2022.

[5] C. N. Yang. The spontaneous magnetization of a two-dimensional ising model. *Phys. Rev.*, 85:808–816, Mar 1952.

[6] Tai Tsun Wu, Barry M. McCoy, Craig A. Tracy, and Eytan Barouch. Spin-spin correlation functions for the two-dimensional ising model: Exact theory in the scaling region. *Phys. Rev. B*, 13:316–374, Jan 1976.

[7] W. K. Hastings. Monte Carlo sampling methods using Markov chains and their applications. *Biometrika*, 57(1):97–109, 04 1970.

[8] M. Nieto Pérez, M. Regal Sevilla, D. Ainoo Pérez, M. Molina O'Brien, L. Mompó Ruiz, and M. Osa Bonillo. Estudio del modelo de Ising en una dimensión empleando simulaciones computacionales. 2023.

[9] Angelica L. Gelover-Santiago. *Simulación del modelo de Ising con el método de Monte Carlo*. Facultad de Ciencias, UNAM, 2005.

[10] Andrea Pelissetto and Ettore Vicari. Critical phenomena and renormalization-group theory. *Physics Reports*, 368, 01 2001.

[11] Ronald Bracewell. *The Fourier Transform and Its Applications*. McGraw-Hill, 2000.